Modulating aqueous solution properties to optimize radiofrequency heating

Nadia C. Lara[1], Jason Chak-shing Ho[2], Lon J. Wilson[1], Andrew R. Barron[1,3,4], Steven A. Curley[2,3], Stuart J. Corr[1,2]

[1] Department of Chemistry and the Richard E. Smalley Institute for Nanoscale Science and Technology, Rice University, Houston, TX 77005, USA

[2] Division of Surgery, Baylor College of Medicine, Houston, TX 77030, USA

[3] Department of Materials Science and Nanoengineering, Rice University, Houston, TX 77005, USA

[4] Energy Safety Research Institute (ESRI), Swansea University Bay Campus, Swansea, SA1 8EN, UK

Exposure to a noninvasive, external radiofrequency (RF) electric field has been proposed for the treatment of cancer, using nanoparticles as heating agents within a tumor. The Kanzius Radiofrequency Hyperthermia system has been proposed for hypothermic therapy of cancer. Studies using this system in combination with gold and carbon-based nanoparticles have sparked much debate regarding the RF heating mechanisms of nanomaterials, especially in conductive, biologically-relevant media. Past research has focused on optimizing nanoparticle properties to enhance energy absorption and nano-localized heat, but no effort has been made to enhance the heating of highly conductive media by directly modulating its bulk dielectric properties. Here we show that simple materials, including salts, sugars, sugar alcohols, and betaines, can be used to modulate the

conductivity of aqueous solutions to optimize their heating rates. These materials are non-toxic, inexpensive, and universally available, and thus highly attractive for clinical use.

Cancer is the second leading cause of mortality in the U.S. and, despite ongoing improvements in the three primary treatment modalities of surgery, chemotherapy, and radiation therapy, five-year survival for certain solid malignancies such as pancreatic and lung cancer remains profoundly low. RF-induced hyperthermia has long been investigated as a treatment modality for cancer but various clinical trials involving its use have produced mixed results[1–10]. One of the hallmark challenges in RF treatment of cancer is sufficiently heating a tumor to the desired temperature while sparing normal tissue, particularly fatty subcutaneous tissue that is prone to over-heating. It has been stated that tumor tissue, owing to its abnormal structure and hence increased electric conductivity, selectively heats more so than normal tissue when exposed to RF[11]. Separately, nanoparticles, especially gold nanoparticles, have been coupled with noninvasive RF to enhance heating and cytotoxicity[12–16], generating much debate on the RF heating mechanism of nanomaterials[17–23]. The presence of salts, especially, in aqueous solutions and biological systems is known to affect the RF heating behavior of gold nanoparticles, but the role of salts may be "the most unresolved aspect of thermal dissipation by gold nanoparticles in RF," according to a recent review[22]. Surfactant-wrapped single-walled carbon nanotubes have also been coupled with RF to enhance heating *in vitro* and *in vivo*[24], similarly motivating a number of experimental and theoretical studies on nanoparticle heating mechanisms[25–28]. The nature of RF heating in biologically relevant materials remains poorly understood. Establishing a solid framework for RF heating in biological materials is needed not only for modeling heating behavior but also for optimization of tissue hyperthermia for therapeutic use. Here we present

well-defined experimental and theoretical heating curves for aqueous salt solutions that in the future will serve as a foundation for understanding the role of salts in nanoparticle heating.

Macroscopic biological materials respond to electromagnetic (EM) fields as governed by their dielectric properties, i.e., permittivity. In time-varying alternating electric fields such as radiofrequency waves, a material's permittivity becomes a complex function as a result of the electric polarization of the medium and is given by the equation:

$$\varepsilon_r = \varepsilon_r' + i\varepsilon_r'' = \varepsilon_r' + i\frac{\sigma}{\omega\varepsilon_0} \qquad (1)$$

where ε_r, ε_r', ε_r'' are the complex, real-valued, and imaginary relative permittivities, respectively, i is $\sqrt{-1}$, σ is the conductivity, ε_0 is the relative permittivity of free space, and ω is the angular frequency. Dielectric materials heat when exposed to electromagnetic fields within the radio- and microwave frequency range (3 kHz–300 GHz) and the energy absorbed by the medium is defined by the specific absorption rate (SAR): $\text{SAR} = \sigma E^2/2\rho$. The rate of heating of a material exposed to EM fields is then:

$$\text{HR} = \frac{\partial T}{\partial t} = \frac{\sigma|E_{\text{eff}}|^2}{2\rho c_p} \qquad (2)$$

where E_{eff} is the effective electric field within the sample, ρ is the mass density and c_p is the specific heat capacity.

Cancerous tissue, by virtue of abnormal cell growth and structure, has intrinsically different dielectric properties than that of normal tissue[11,29–32]. This difference in permittivity, it has been postulated, can be exploited to selectively heat and thus injure cancerous cells while leaving normal tissue intact. A common mistake in interpreting equation (2), however, is to simply equate higher conductivity with increased heating rate[15,25]. An external, applied electric

field E_{app}impinging upon an interface of two dielectric materials must obey the following boundary condition:

$$\varepsilon_{r,1}E_{\text{app}} = \varepsilon_{r,2}E_{\text{eff}} \qquad (3)$$

in which it becomes apparent that the ratio of dielectric properties at the interface influences the effective electric field within the material of interest. In the case of pure water surrounded by air, the ratio $\varepsilon_{r,\text{air}}/\varepsilon_{r,\text{sample}}$ is on the order of 10^{-2} and the ratio is 10^{-4} for normal sodium chloride (physiologic saline) surrounded by air. In the latter case, saline is greatly polarized by the applied electric field, thus reducing the internal effective electric field experienced by the bulk media. Accounting for the boundary condition allows for a more precise heating rate model of a sample surrounded by air, as is the case in the experiments reported here:

$$\text{HR} = \frac{\sigma\left|\frac{\varepsilon_{r,\text{air}}}{\varepsilon_r}E_{\text{app}}\right|^2}{2\rho c_p} \qquad (4)$$

where $\varepsilon_{r,\text{air}}$ and ε_r are the absolute relative permittivities of air and the sample, respectively. This model results in a theoretical and experimentally confirmed peak heating rate of saline solution with concentration of 5.6 mM corresponding to a conductivity of 0.06 S/m at a frequency of 13.56 MHz[33,34]. Herein we generalize this heating model to that of a large variety of salts and show that maximal heating occurs at the same conductivity of 0.06 S/m regardless of the atomic or molecular identity of salts.

RF heating of aqueous salt solutions

We measured the RF heating rates of an assortment of salts dissolved in ultra-pure water in the concentration range 0.01–200 mM. The salts tested were NaCl, $NaC_2H_3O_2$, $MgCl_2$, Na_2SO_4, $AuCl_3$, and $Na_3C_6H_5O_7$ (sodium citrate). Samples were loaded onto a 1.3 mL non-

conductive quartz cuvette and exposed to a RF field (13.56 MHz operating frequency) at 100 W generator power (Fig. 1a). Sample temperature was measured using an infrared camera and the heating rates were calculated by a least-squares linear regression of the resultant temperature-time plot (Fig. 1b). Samples were heated from 23 °C to either 27 °C or for a duration of 60 s, whichever occurred first. Over this selected small temperature range, the variation of heating rate of the solutions due to the temperature-dependence of dielectric properties is estimated to be less than 0.07%. Each salt displays a characteristic peak heating curve as a function of concentration (Fig. 2a), with salts of greater valence typically displaying peak heating at lower concentrations than salts of lesser valence.

The heating curves for the individual salt solutions collapse into a single curve when the conductivity of solutions is considered as shown in Fig. 2b. Peak heating occurred for all measured salts at a conductivity of 0.060 S/m. We obtained conductivity values at 13.56 MHz (RF generator operating frequency) of each sample by measuring their complex relative permittivity (ε_r' and σ) in the range 10 MHz–3 GHz. Of note, when measuring the relative permittivity of highly conductive solutions, electrode polarization occurs at low frequencies, which can result in significant instrument-related measurement errors, especially for ε_r' [17]. We have performed the necessary corrections[25] and found these errors to be insignificant (<1.2% for σ and ε_r) for our purposes in the conductivity range studied (Extended Data Fig. 1c). The heating model of saline is thus generalized to all salts by demonstrating that the heating rate of salts is dependent on bulk conductivity regardless of specific atomic or molecular identity.

Enhancing RF heating of ionic solutions

From the generalized RF heating curve for salts, it is apparent that an increase in material conductivity does not monotonically increase heating rate. Peak heating for aqueous media occurs at a conductivity of 0.060 S/m, beyond which addition of conductive material will decrease heating rate. Indeed, this was shown using metallic and semiconducting carbon nanotubes, though this behavior was not yet well understood[27]. Blood and body fluids are present on the far right of the curve with conductivities of 1.1 and 1.5 S/m, respectively, at 13.56 MHz[35]. Intra- and extra-cellular environments of cells have similarly high ion content. Therefore, increasing the heating rate of body tissues under RF energy would require *diluting* existing ionic content, a task not readily performable or tolerated *in vivo*.

An alternative approach presented herein is to introduce neutral, water-soluble materials called kosmotropes that, when added to an ionic aqueous solution, serve to decrease conductivity and thus increase RF heating rate of the solution. Kosmotropic ("structure-forming") materials preferentially interact with water solvent molecules and form hydrogen bonds to water that are stronger than the water-water hydrogen bonds, thus stabilizing the water network[36]. Glycerol, propylene glycol, ethylene glycol, and methanol are examples of kosmotropes that are used as anti-freeze agents; in nature, sugars such as trehalose and sucrose act as cryo-protective agents when present in high concentrations in flora and fauna. Biotechnologists commonly use dimethylsulfoxide as their cryoprotectant agent of choice to reduce cellular damage by ice when freezing cells for long-term storage. Marine life, such as seagrasses, use a wide variety of kosmotropic materials, such as sugars, sugar alcohols, and zwitterions to maintain osmotic balance in the rapidly changing salinity of seawater[37]. Quaternary ammonium compounds called betaines, also in high concentrations, allow bacteria to survive in highly ionic environments. For example, glycine betaine is used by *E. coli* to counteract the effects of low pH and high urea

concentrations in the urinary tract[38]. In stabilizing the water network, these materials can also reduce ion mobility, a property we exploit to reduce the conductivity of highly ionic solutions thereby increasing their heating rate accordingly. To our knowledge, this is the first time that RF heating rates of aqueous solutions have been modulated in this way.

To perform the experiment, we measured the RF heating rates and complex permittivities of a number of kosmotropes (Fig 3a) dissolved in phosphate buffered saline (PBS), a biologically iso-osmolar solution with similar conductivity (1.15 S/m) to blood and body tissues. The kosmotropes tested were sucrose, maltose, glucose, ethylene glycol, propylene glycol, glycerol, sorbitol, glycine, sarcosine, glycine betaine, and dimethylsulfoxide. Kosmotrope solutions in PBS were prepared and appropriately diluted from concentrated stock PBS (10x PBS containing 90 g/L NaCl, 1.44 g/L KH_2PO_4, and 7.95 g/L Na_2HPO_4) to maintain equivalent final ionic concentrations in all solutions. RF heating rates and complex permittivity were measured in the same fashion as the salt heating experiments described above. We found that all of the kosmotropic materials tested decreased the conductivity of PBS and increased its heating rate in a concentration-dependent manner as shown in Fig. 3b. Propylene glycol outperformed all other materials at every concentration studied, increasing the heating rate of PBS by 490% when added at a concentration of 500 mg/mL. On average, PBS heating rate increased from 0.028 °C/s to 0.034 ± 0.001, 0.052 ± 0.001, and 0.112 ± 0.004 °C/s at kosmotrope concentrations of 100, 250, and 500 mg/mL, respectively. Regardless of concentration, kosmotrope-PBS solutions heat similarly to salt solutions of the same conductivity, according to the same heating model when exposed to the RF field.

From equation (4), it is clear that heating rate can also be manipulated by altering heat capacity and density. For example, we found that lithium chloride displayed peak heating rates of

0.37, 0.67, and 1.21 °C/s when dissolved in pure water, 70% ethanol, and pure ethanol, respectively (Fig. 3d). The increase in peak heating rate with increasing ethanol content corresponds to decreases in heat capacity, density, and ε_r' of the solvent. Although systemic administration of pure ethanol would not be physiologically tolerated, direct injection of ethanol into tumors is already used therapeutically in hepatic arterial chemo-embolization, which could be coupled with RF hyperthermia therapy.

Modeling RF heating behavior

Thus far we have compared the theoretical model to experimental measurements not only for the conductivity at which peak heating occurs in a given aqueous solution, but also the general shape of the curve and found excellent agreement between the two when sample temperature is properly accounted for. We have not, however, made direct comparisons between theoretically predicted and experimentally measured heating rates. For that comparison, all variables in equation (4) must be measured. Unfortunately, it is notoriously difficult to measure the external electric field when the field strength is extremely strong as it is in our experiments. Attempts to measure the field with a voltage probe have led to rapid (< 1 second) overheating and subsequent damage of the probe, even at an RF generator power of 10 W. Instead, we estimate E_{app} by fitting the heating rate model to the salt heating data in Fig. 1b. This calculation requires a further adjustment for the effective electric field term to account for sample holder geometry[39]:

$$E_{\text{eff}} = \frac{1}{1 + N\left(\frac{\varepsilon_r}{\varepsilon_{r,\text{air}}} - 1\right)} E_{\text{app}} \qquad (5)$$

where N is the polarization tensor, $\varepsilon_{r,\text{air}}$ is the relative permittivity of air, and E_{app} is the applied electric field in air. The polarization tensor depends upon the dimensions of the sample and is

approximately 0.596 in the case of our cylindrical cuvette[40]. Note that in the limit where the two materials are geometrically infinite plane layers, N is equal to 1 and E_{eff} reduces to equation (3). We fit equation (2) with the geometry-adjusted expression for E_{eff} shown in equation (5) to the heating rate (HR) and complex permittivity (σ and ε_r) values, using E_{app} as the fit parameter. The heating rate model fit is indicated by the solid line in Fig. 2b. The angular frequency $\omega = 2\pi f$ corresponds to the 13.56 MHz operating frequency of the RF generator and ρ and c_p are estimated to be equal to the values of pure water at 25 °C. Using these parameters, we calculate E_{app} to be 0.49 MV/m at 100 W operating power. Although this value appears to be very large, it is necessary to achieve the heating rates reported. The same heating rate model can be applied to the 13.56 MHz RF system reported by Liu, *et al.*, who reported a maximum temperature increase of only 0.7 °C over an RF exposure period of 10 min (0.00117 °C/s). Based on the sample dimensions given, we estimate N for this system to be 0.673 and calculate E_{app} to be 30.3 kV/m, in excellent agreement with the electric field strength estimated by the authors from low power measurements[34].

Prior studies with the Kanzius RF generator by our group utilized a power settings of 900-1000 W[13,21,24,27,41], compared to 100 W in the study described above. The reason for the reduction in power is to minimize the effects of the aforementioned temperature-dependence of permittivity, in which the heating rate itself would change as the sample material increased in temperature. The further evaluate this phenomenon, we additionally measured RF heating rates of salt solutions at 900 W from 25 °C to 70 °C, or for a duration 120 seconds, whichever occurred first, similar to the experimental conditions we have reported previously. Under these conditions, we measured heating rates as fast as 3.98 °C/s, corresponding to a rise in sample temperature from room temperature (~25 °C) to over 60 °C over a RF exposure period of only

ten seconds. Over this large temperature range, the temperature-dependence of dielectric properties of salt solutions cannot be ignored. Due to this effect, peak heating occurred at lower concentrations (Fig. 4a) and lower conductivity, 0.038 S/m (Fig. 4b), compared to 0.060 S/m at 100 W.

In general, peak heating occurs when the medium's real and imaginary permittivities, ε_r' and ε_r'', respectively, are equal. Both are frequency- and temperature-dependent. For this reason, we cannot fit the heating rate model described by equations (2) and (5) as was done for the heating and permittivity data at 100 W. Instead, we use temperature corrections[42–44] for the conductivity, permittivity, density, and heat capacity of saline solutions to calculate the instantaneous heating rates of saline for any given temperature and concentration. The calculated heating curves at 25, 45, and 70 °C given an estimated applied electric field of 1.53 MV/m are shown in Fig. 4b as a function of solution conductivity at 25 °C. These results show that the average heating rates measured over the temperature range 25–70 °C are similar to the instantaneous heating rates at 45 °C. Other authors have also reported fast heating rates (~1.3 °C/s) that similarly necessitate high electric field strengths[45].

Discussion

RF-induced hyperthermia has gained interest as a compelling treatment modality for cancer. Although knowledge of tissue dielectric properties has accumulated in the past few decades, the behavior of RF heating of biological materials has been not been well characterized and has posed a significant barrier against therapeutic optimization of this potential treatment modality. *In vitro*, prior studies have characterized the heating behavior of saline solutions alone. Here, we have generalized that theoretical heating model to a diverse assortment of salts and

shown that the RF heating behavior is determined by the dielectric and thermal properties of the bulk solution independent of the atomic or molecular identity of the salt. With well-defined experimental and theoretical peak heating curves, we have shown that the heating behavior of aqueous solutions in a RF field is calculated with a relatively simple model even over large temperature ranges once geometry and temperature-dependent properties are well accounted for.

The heating rate model predicts peak heating to occur at a specific bulk medium conductivity for a given frequency as opposed to a monotonic increase with conductivity, a misconception sometimes encountered in the literature. Beyond this peak heating conductivity, heating rate decreases due to the diminished effective field strength within the sample. At 13.56 MHZ, the dielectric properties of biological systems exceed this peak heating value and thus preclude the practice of adding more salts or polar materials, as this addition would actually decrease the heating rate of the medium. To achieve increased heating rates in physiologic materials, we propose the use of kosmotropes such as propylene glycol, sucrose, and glycine betaine, which are a class of molecules that stabilize water structure and decrease the conductivity of highly ionic solutions. We have shown that kosmotropes can be added to physiologic media to increase the heating rate of biologically relevant aqueous solutions in a concentration-dependent manner. In converting this technique into a clinical application, an adequate method for tumor-targeted delivery of these materials will need to be identified. One possibility includes percutaneous arterial injection into the local tumor vasculature, similar to the well-known and clinically available technique of arterial chemo-embolization. The human body, however, is complex dielectric with many tissue interfaces, therefore the effects of kosmotropes on the RF heating rates of *in vivo* tissues will need to be investigated. Most of the substances tested here for RF heating enhancement are widely available, inexpensive, and considered safe

when ingested in moderate quantities, making them highly attractive for clinical use. We believe that with further understanding of suitable kosmotropes the availability of RF-induced hyperthermia can become a treatment universal and not limited by the cost of “designer” drugs.

Materials and Methods

Sample preparation

Aqueous salt solutions were prepared in high-resistivity water (18.2 MΩ/cm) using a number of monovalent (KCl, LiCl, NaBr, NaCl, $NaC_2H_3O_2$, NaI, $NaNO_3$), divalent ($BaCl_2$, $CaCl_2$, $MgCl_2$, Na_2CO_3, Na_2SO_4), and trivalent salts ($AuCl_3$, $GdCl_3$, $Na_3C_6H_5O_7$, and Na_3PO_4) at concentrations varying from 0.001 mM to 2 M. For kosmotrope experiments, 1 mL of concentrated PBS containing 90 g/L NaCl, 1.44 g/L KH_2PO_4, and 7.95 g/L Na_2HPO_4 was added to a known mass of kosmotrope material, followed by dilution to 10 mL to ensure equal ion concentration across all samples. Kosmotrope materials (sucrose, maltose, trehalose, glycerol, propylene glycol, ethylene glycol, glycine betaine, dimethylsulfoxide) and all salts were obtained from Sigma-Aldrich in high purity (>98 %) and used as received.

Electrical characterization

Complex permittivity measurements were taken using an Agilent 85070E high-temperature coaxial dielectric probe (Agilent Technologies, Santa Clara, CA) connected to an Agilent E4991A impedance analyzer to extend the frequency range of the probe down to 10 MHz. Four-point calibration (open, short, 50 ohm load, low-loss capacitor) of the impedance analyzer was performed prior to each measurement session. Three-point probe calibration of the probe (air, short, water) was performed periodically between samples and a single-point calibration (air) was performed between every sample to eliminate signal drift. For measurements, 600 μL of sample was loaded onto the probe and approximately 400 logarithmic data points were acquired across the frequency range 10 MHz–3 GHz with each measurement performed in triplicate in rapid succession to avoid probe drift. We found no difference between loading a small amount of sample onto probe and immersing the probe into a plastic beaker

containing 20 mL of sample. Additionally, for each sample in the 900 W experiment, static solution DC conductivity was measured ten times using either an InLab 731 or 741 conductivity probe (Mettler Toledo, Columbus, OH), depending on the conductivity of the sample and the measurement range of each probe (data not shown). DC conductivity measurements were in agreement with AC conductivity measurements performed using the impedance analyzer at 13.56 MHz.

Radiofrequency heating

A variable power Kanzius External RF (13.56 MHz) Generator System (ThermMed, LLC, Erie, PA) was used to heat aqueous solutions. A high-voltage RF field is generated in the 8 cm air gap between the transmitting and receiving heads of the RF-field generator. For aqueous experiments, samples were placed in a 1.3 mL quartz cuvette on a non-conducting Teflon holder mounted on an adjustable rotary stage at ambient temperature and open to air. The cuvette was placed 8 mm from the transmitting head of the RF-field generator and exposed to the high-voltage RF field at 100 or 900 W generator power. Sample temperatures were recorded using an infrared camera (FLIR SC 6000, FLIR Systems, Inc., Boston, MA) approximately every 0.17 s. At 100 W, samples were heated from ambient temperature (~23 °C) to 27 °C or for a duration of 60 s, whichever occurred first. At 900 W, samples were heated from ambient temperature to 70 °C or for a duration of 120 s, whichever occurred first. Heating rates were calculated by fitting a linear regression to the temperature versus time plot of each sample for the duration of RF exposure.

References

1. Hiraoka, M. *et al.* Development of RF and microwave heating equipment and clinical applications to cancer treatment in Japan. *IEEE Trans. Microw. Theory Techn.* **48,** 1789–1799 (2000).
2. De Haas-Kock, D. F. M. *et al.* Concomitant hyperthermia and radiation therapy for treating locally advanced rectal cancer. *Cochrane Db. Syst. Rev.* CD006269 (2009). doi:10.1002/14651858.CD006269.pub2
3. Zagar, T. M. *et al.* Hyperthermia combined with radiation therapy for superficial breast cancer and chest wall recurrence: a review of the randomised data. *Int. J. Hyperthermia* **26,** 612–617 (2010).
4. Van der Zee, J. *et al.* Comparison of radiotherapy alone with radiotherapy plus hyperthermia in locally advanced pelvic tumours: a prospective, randomised, multicentre trial. Dutch Deep Hyperthermia Group. *Lancet* **355,** 1119–1125 (2000).
5. Vasanthan, A. *et al.* Regional hyperthermia combined with radiotherapy for uterine cervical cancers: a multi-institutional prospective randomized trial of the international atomic energy agency. *Int. J. Radiat. Oncol.* **61,** 145–153 (2005).
6. Mitsumori, M. *et al.* Regional hyperthermia combined with radiotherapy for locally advanced non-small cell lung cancers: a multi-institutional prospective randomized trial of the International Atomic Energy Agency. *Int. J. Clin. Oncol.* **12,** 192–198 (2007).
7. Ohguri, T. *et al.* Radiotherapy with 8-MHz radiofrequency-capacitive regional hyperthermia for stage III non-small-cell lung cancer: the radiofrequency-output power correlates with the intraesophageal temperature and clinical outcomes. *Int. J. Radiat. Oncol.* **73,** 128–135 (2009).

8. Perez, C. A. *et al.* Randomized phase III study comparing irradiation and hyperthermia with irradiation alone in superficial measurable tumors. Final report by the Radiation Therapy Oncology Group. *Am. J. Clin. Oncol.* **14,** 133–141 (1991).
9. Harima, Y. *et al.* A randomized clinical trial of radiation therapy versus thermoradiotherapy in stage IIIB cervical carcinoma. *Int. J. Hyperthermia* **17,** 97–105 (2001).
10. Jones, E. L. *et al.* Randomized trial of hyperthermia and radiation for superficial tumors. *J. Clin. Oncol.* **23,** 3079–3085 (2005).
11. Raoof, M. *et al.* Tumor selective hyperthermia induced by short-wave capacitively-coupled RF electric-fields. *PLOS ONE* **8,** e68506 (2013). DOI: 10.1371/journal.pone.0068506
12. Cardinal, J. *et al.* Noninvasive radiofrequency ablation of cancer targeted by gold nanoparticles. *Surgery* **144,** 125–132 (2008).
13. Gannon, C. J., Patra, C. R., Bhattacharya, R., Mukherjee, P. & Curley, S. A. Intracellular gold nanoparticles enhance non-invasive radiofrequency thermal destruction of human gastrointestinal cancer cells. *J. Nanobiotechnology* **6,** 2 (2008).
14. Curley, S. A. *et al.* Noninvasive radiofrequency field-induced hyperthermic cytotoxicity in human cancer cells using cetuximab-targeted gold nanoparticles. *J. Exp. Ther. Oncol.* **7,** 313–26 (2008).
15. Moran, C. H. *et al.* Size-dependent joule heating of gold nanoparticles using capacitively coupled radiofrequency fields. *Nano Res.* **2,** 400–405 (2009).
16. Glazer, E. S. *et al.* Noninvasive radiofrequency field destruction of pancreatic adenocarcinoma xenografts treated with targeted gold nanoparticles. *Clin. Cancer Res.* **16,** 5712–5721 (2010).

17. Hanson, G. W. & Patch, S. K. Optimum electromagnetic heating of nanoparticle thermal contrast agents at rf frequencies. *J. Appl. Phys.* **106,** 054309 (2009).
18. Li, D. *et al.* Negligible absorption of radiofrequency radiation by colloidal gold nanoparticles. *J. Colloid Interface Sci.* **358,** 47–53 (2011).
19. Hanson, G. W., Monreal, R. C. & Apell, S. P. Electromagnetic absorption mechanisms in metal nanospheres: bulk and surface effects in radiofrequency-terahertz heating of nanoparticles. *J. Appl. Phys.* **109,** 124306 (2011).
20. Liu, X., Chen, H., Chen, X., Parini, C. & Wen, D. Low frequency heating of gold nanoparticle dispersions for non-invasive thermal therapies. *Nanoscale* **4,** 3945–3953 (2012).
21. Corr, S. J. *et al.* Citrate-capped gold nanoparticle electrophoretic heat production in response to a time-varying radio-frequency electric field. *J. Phys. Chem. C* **116,** 24380–24389 (2012).
22. Collins, C. B., McCoy, R. S., Ackerson, B. J., Collins, G. J. & Ackerson, C. J. Radiofrequency heating pathways for gold nanoparticles. *Nanoscale* **6,** 8459–8472 (2014).
23. Liu, X. *et al.* Radiofrequency heating of nanomaterials for cancer treatment: Progress, controversies, and future development. *Appl. Phys. Rev.* **2,** 011103 (2015).
24. Gannon, C. J. *et al.* Carbon nanotube-enhanced thermal destruction of cancer cells in a noninvasive radiofrequency field. *Cancer* **110,** 2654–2665 (2007).
25. Gach, H. M. & Nair, T. Radiofrequency interaction with conductive colloids: permittivity and electrical conductivity of single-wall carbon nanotubes in saline. *Bioelectromagnetics* **31,** 582–588 (2010).
26. Nair, T., Symanowski, J. T. & Gach, H. M. Comparison of complex permittivities of isotonic colloids containing single-wall carbon nanotubes of varying chirality. *Bioelectromagnetics* **33,** 134–146 (2012).

27. Corr, S. J. *et al.* Radiofrequency electric-field heating behaviors of highly enriched semiconducting and metallic single-walled carbon nanotubes. *Nano Res.* (2015). doi:10.1007/s12274-015-0791-1
28. Shuba, M. V., Slepyan, G. Y., Maksimenko, S. A. & Hanson, G. W. Radiofrequency field absorption by carbon nanotubes embedded in a conductive host. *J. Appl. Phys.* **108,** 114302 (2010).
29. Wang, H. *et al.* Dielectric properties of human liver from 10 Hz to 100 MHz: normal liver, hepatocellular carcinoma, hepatic fibrosis and liver hemangioma. *Bio-Med. Mater. Eng.* **24,** 2725–2732 (2014).
30. Lazebnik, M. *et al.* A large-scale study of the ultrawideband microwave dielectric properties of normal, benign and malignant breast tissues obtained from cancer surgeries. *Phys. Med. Biol.* **52,** 6093–6115 (2007).
31. Joines, W. T., Zhang, Y., Li, C. & Jirtle, R. L. The measured electrical properties of normal and malignant human tissues from 50 to 900 MHz. *Med. Phys.* **21,** 547–550 (1994).
32. Surowiec, A. J., Stuchly, S. S., Barr, J. B. & Swarup, A. Dielectric properties of breast carcinoma and the surrounding tissues. *IEEE Trans. Biomed. Eng.* **35,** 257–263 (1988).
33. Griffiths, H., Ahmed, A. & Smith, C. Power loss in skin cooling pillows during RF hyperthermia. *Br. J. Radiol.* **57,** 254–256 (1984).
34. Liu, X. *et al.* Conductivity and frequency dependent specific absorption rate. *J. Appl. Phys.* **113,** 074902 (2013).
35. Gabriel, S., Lau, R. W. & Gabriel, C. The dielectric properties of biological tissues: III. Parametric models for the dielectric spectrum of tissues. *Phys. Med. Biol.* **41,** 2271–2293 (1996).

36. Galinski, E. A., Stein, M., Amendt, B. & Kinder, M. The kosmotropic (structure-forming) effect of compensatory solutes. *Comp. Biochem. Physiol. A* **117,** 357–365 (1997).
37. Touchette, B. W. Seagrass-salinity interactions: physiological mechanisms used by submersed marine angiosperms for a life at sea. *J. Exp. Mar. Biol. Ecol.* **350,** 194–215 (2007).
38. Chambers, S. T., Peddie, B. A., Randall, K. & Lever, M. Inhibitors of bacterial growth in urine: what is the role of betaines? *Int. J. Antimicrob. Ag.* **11,** 293–296 (1999).
39. Li, D. *et al.* The effect of sample holder geometry on electromagnetic heating of nanoparticle and NaCl solutions at 13.56 MHz. *IEEE Trans. Biomed. Eng.* **59,** 3468–3474 (2012).
40. Portis, A. M. *Electromagnetic Fields: Sources and Media*. (Wiley, New York, 1978).
41. Raoof, M. *et al.* Stability of antibody-conjugated gold nanoparticles in the endolysosomal nanoenvironment: implications for noninvasive radiofrequency-based cancer therapy. *Nanomedicine* **8,** 1096–1105 (2012).
42. Stogryn, A. Equations for calculating dielectric constant of saline water. *IEEE Trans. Microw. Theory Techn.* **19,** 733–736 (1971).
43. Kaatze, U. Complex permittivity of water as a function of frequency and temperature. *J. Chem. Eng. Data* **34,** 371–374 (1989).
44. Haynes, W. M., ed. 'Thermophysical properties of water and steam' in *CRC Handbook of Chemistry and Physics, 96th Edition*. (CRC Press/Taylor and Francis, Internet Version 2015).
45. Kruse, D. E. *et al.* A radio-frequency coupling network for heating of citrate-coated gold nanoparticles for cancer therapy: design and analysis. *IEEE Trans. Biomed. Eng.* **58,** 2002–2012 (2011).

Acknowledgements

This material is based upon work supported by the National Science Foundation Graduate Research Fellowship Program under Grant No. 1450681 and is also supported by an unrestricted research grant from the Kanzius Research Foundation (SAC, Erie, Pennsylvania). A.R.B. is supported by the Welsh Government Sêr Cymru Programme and the Robert A. Welch Foundation (C-0002). N. C. L would like to thank Asad Haider for assistance in obtaining preliminary data.

Author Contributions

N.C.L. collected and analyzed data and wrote the paper; N.C.L., S.J.C., L.J.W., and S.A.C. designed the salt heating study; N.C.L. and A.R.B. designed the kosmotrope study; J.C.H. was involved in data analysis and manuscript editing. All authors discussed the results and commented on the manuscript.

Author Information

Reprints and permissions information is available at www.nature.com/reprints. The authors report no conflicting financial interest. Correspondence and request for materials should be addressed to S.J.C. (stuart.corr@bcm.edu) Any opinions, findings, and conclusions or recommendations expressed in this material are those of the authors and do not necessarily reflect the views of the National Science Foundation.

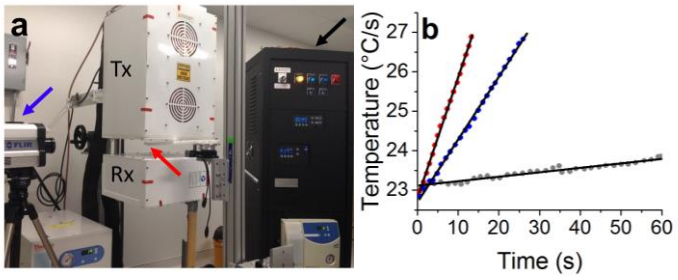

Figure 1 | Experimental setup for the RF-Induced heating of aqueous solutions. a, The non-invasive Kanzius RF system. A radiofrequency (13.56 MHz) generator (black arrow) is used to generate a high-voltage electric field between the transmitting (Tx) and receiving (Rx) heads. An infrared camera (blue arrow) is used to record the temperature of the sample (red arrow). **b,** Temperature plots for 0.1 (grey), 1 (blue), and 10 mM (red) NaCl solutions. Least-squares linear regressions (solid lines) are used to calculate RF heating rates. Insert displays the IR camera view of the sample.

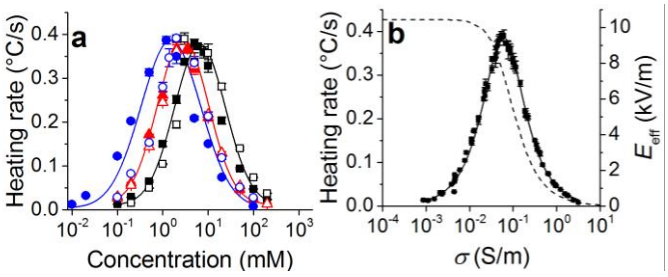

Figure 2 | RF heating of salt solutions. a, Concentration-dependent heating at 100 W of monovalent (black; NaCl - ■, $NaC_2H_3O_2$ - □), divalent (red; $MgCl_2$ - ▲, Na_2SO_4 - △), and trivalent salts (blue; $AuCl_3$ - ●, $Na_3C_6H_5O_7$ - ○). **b,** Conductivity dependence of heating rates (■) and effective electric field (dashed line). Black line indicates heating rate model fit described by equations (2) and (5). Heating rates reported are averages of three replicates with error bars indicating SEM.

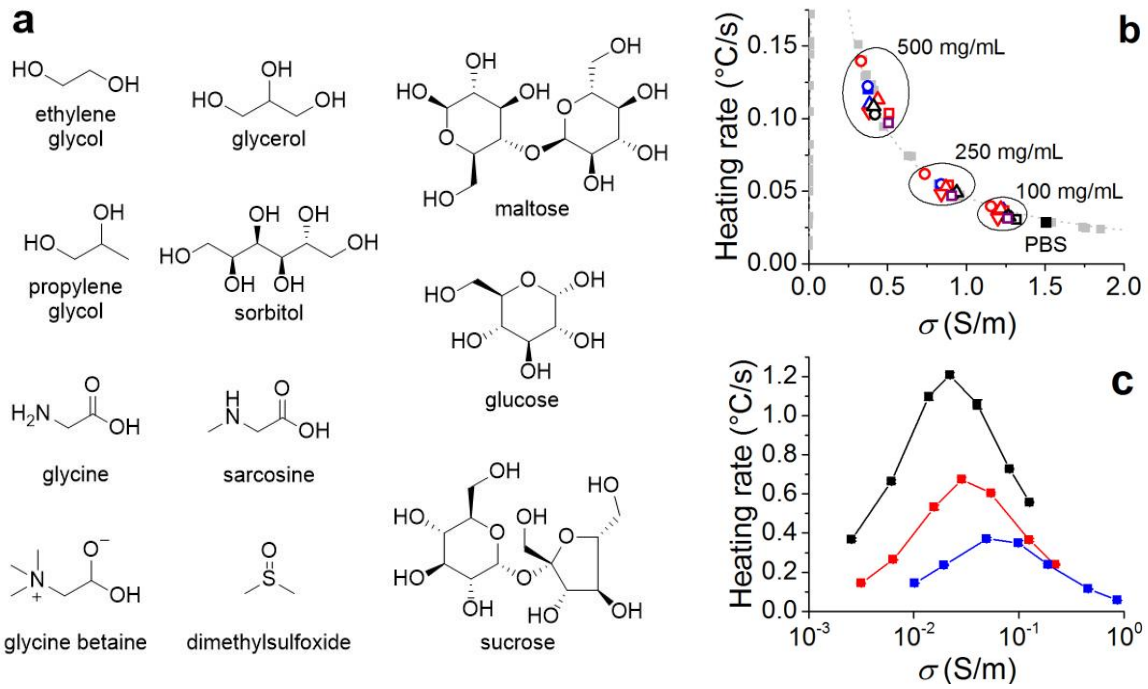

Figure 3 | Modulating solution properties to optimize RF heating. a, Kosmotrope structures. **b,** Kosmotropes enhance the heating rate of PBS (■) in a concentration-dependent manner. Kosmotropes include sugar alcohols (red; ethylene glycol - □, propylene glycol - ○, glycerol - △, sorbitol - ▽), sugars (blue; maltose - □, glucose - ○, sucrose - △), amines (black; glycine - □, sarcosine - ○, glycine betaine - △), and dimethylsulfoxide (purple, □). Salt solution heating from Fig. 2b is shown in grey. **c,** Heating rates of LiCl in ethanol (black), 70% ethanol (red), and water (blue) at 1–100 mM. All heating rates are averages of three replicates. Error bars indicating SEM are omitted for clarity in **b** but are generally smaller than symbols.

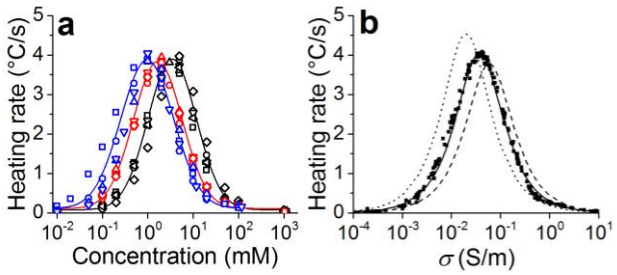

Figure 4 | RF heating of salt solutions at high power. a, Concentration-dependent heating at 900 W of monovalent (black; KCl - □, LiCl - ○, NaBr - △, NaCl - ▽, $NaC_2H_3O_2$ - ◇, NaI - ◁), divalent (red; $BaCl_2$ - □, $CaCl_2$ - ○, $MgCl_2$ - △, Na_2CO_3 - ▽, Na_2SO_4 - ◇), and trivalent salts (blue; $AuCl_3$ - □, $GdCl_3$ - ○, $Na_3C_6H_5O_7$ - △, Na_3PO_4 - ▽). **b,** Measured (■) and calculated (lines) heating rates of saline at 25 (dotted), 45 (solid), and 70 (dashed) °C. Heating rates reported are averages of three replicates. Error bars indicating SEM are omitted for clarity but are generally smaller than symbols.

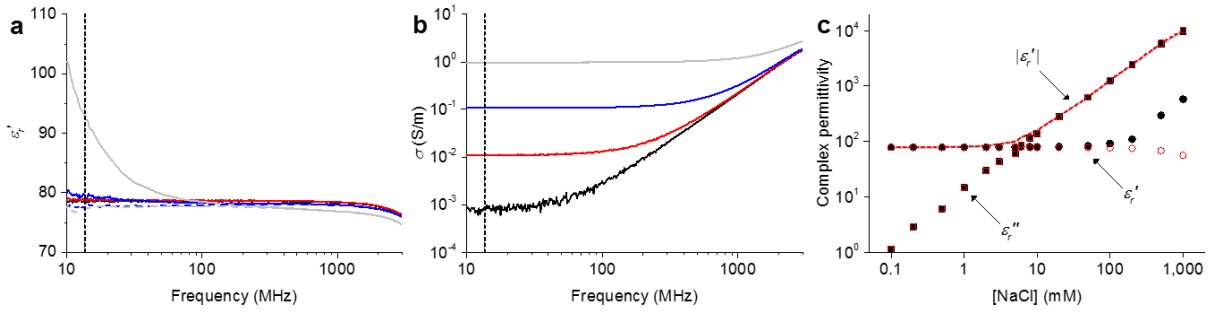

Extended Data Figure 1 | Complex permittivity of NaCl. a, Real-valued permittivity and **b,** conductivity of 0.1 (black), 1 (red), 10 (blue), and 100 (grey) mM NaCl over the frequency range 10 MHz–3 GHz. Dashed blue and grey lines indicate low frequency polarization correction of real-valued permittivity of 10 and 100 mM NaCl, respectively. Dotted black line indicates 13.56 MHz. **c,** Concentration-dependence of ε_r' (circles) and ε_r'' (squares) for NaCl at 13.56 MHz, both measured (black) and corrected (red) values are shown. The absolute value of the relative permittivity $|\varepsilon_r|$ is indicated for measured (grey line) and corrected (dotted red line) values.